

and the EMT type structure. Like the superstructure in faujasite, the large cage in UCSB-10 is bound with four 12-rings tetrahedrally distributed. The structure of UCSB-10 can be obtained from the faujasite type by replacing the sodalite cage with the one-sided capped cancrinite cage. Such a relation becomes obvious if a rhombohedral unit cell is used to describe the cubic faujasite structure. For example, the cubic cell of a faujasite analog, CAP-FAU1, can be transformed into a rhombohedral cell with $a = 17.54 \text{ \AA}$ and $c = 42.95 \text{ \AA}$, which becomes very similar to the unit cell of UCSB-10Co ($a = 17.70 \text{ \AA}$, $c = 41.69 \text{ \AA}$). A noticeable difference is that faujasite and EMT structures have c axes that are more than 1 \AA longer than those of the corresponding UCSB-6 and UCSB-10 structures. This difference has allowed the screening of a large number of crystals grown under various synthesis conditions by determination of unit cell parameters only.

Future directions. The compositional domains achieved in this study imply that there might exist a large family of zeolite type structures not yet synthesized. Some of these unknown phases should be accessible with use of the approach developed here. Such work could open up new areas of research in the synthesis of zeolite type materials. The availability of large single crystals for many related large-pore structures containing different metal cations and protonated amines provides an opportunity to study in detail the coordination chemistry of metal atoms in the zeolite type framework and the structure-directing effects of amines, which should provide guidance for the future design of molecular sieves. The observed correlation between pore geometry and framework charge density is supported by the successful synthesis of UCSB-6, UCSB-8, and UCSB-10 structures with a variety of chemical compositions. It is suggested that a design strategy that allows the expansion of the cage-like structural subunits can lead to even larger cages and a lower framework T-atom density.

REFERENCES AND NOTES

- W. M. Meier, D. H. Olson, Ch. Baerlocher, *Atlas of Zeolite Structure Types* (Elsevier, Boston, MA, 1996); H. van Bekkum, E. M. Flanigen, J. C. Jansen, Eds., *Introduction to Zeolite Science and Practice* (Elsevier, Amsterdam, 1991); D. W. Breck, *Zeolite Molecular Sieves* (Wiley, New York, 1974).
- M. E. Davis, C. Saldarriaga, C. Montes, J. Garces, C. Crowder, *Nature* **331**, 698 (1988); R. M. Dessan, J. L. Schlenker, J. B. Higgins, *Zeolites* **10**, 552 (1990); C. C. Freyhardt, M. Tsapatsis, R. F. Lobo, K. J. Balkus Jr., M. E. Davis, *Nature* **381**, 295 (1996).
- R. H. Richard *et al.*, *J. Solid State Chem.* **102**, 204 (1993); M. Estermann, L. B. McCusker, C. Baerlocher, A. Merrouche, H. Kessler, *Nature* **352**, 320 (1991).
- M. I. Khan *et al.*, *Chem. Mater.* **8**, 43 (1996).
- T. R. Gaffney, *Curr. Opin. Solid State Mater. Sci.* **1**, 69 (1996).
- L. B. McCusker, in *Comprehensive Supramolecular Chemistry*, G. Alberti and T. Bein, Eds. (Elsevier, New York, 1996), vol. 7, pp. 393–423.
- P. Feng, X. Bu, G. D. Stucky, *Nature* **388**, 735 (1997).
- M. E. Davis and S. I. Zones, in *Synthesis of Porous Materials, Zeolites, Clays, and Nanostructures*, M. L. Occelli and H. Kessler, Eds. (Dekker, New York, 1996), pp. 1–34.
- J. M. Bennett and B. K. Marcus, in *Innovation in Zeolite Materials Science*, P. J. Grober, W. J. Mortier, E. F. Vansant, G. Schulz-Ekloff, Eds. (Elsevier, New York, 1980), pp. 269–279; P. A. Wright *et al.*, *J. Chem. Soc. Chem. Commun.* **1993**, 633 (1993).
- P. Feng, X. Bu, G. D. Stucky, *Angew. Chem. Int. Ed. Engl.* **34**, 1745 (1995).
- Q. Huo *et al.*, *Science* **268**, 1324 (1995).
- Diamines, $\text{NH}_2(\text{CH}_2)_n\text{NH}_2$ ($7 \leq n \leq 12$), have been used for some time in the synthesis of microporous materials and are known to be the structure-directing agents in the crystallization of multidimensional high-silica zeolites ZSM-5 and ZSM-11 [E. W. Vallyocik and L. D. Rollmann, *Zeolites* **5**, 123 (1985)].
- S. T. Wilson and E. M. Flanigen, in *Zeolite Synthesis*, M. L. Occelli and H. E. Robson, Eds. (ACS Symposium Series 398, American Chemical Society, Washington, DC, 1989), pp. 329–345.
- The crystal structure of MnPO_4 -11 was reported; however, the concentration of Mn is too low to have an effect on the structural refinement [J. J. Pluth *et al.*, *J. Phys. Chem.* **92**, 2734 (1988)].
- H. Kessler, J. Patarin, C. Schott-Darie, in *Studies in Surface Science and Catalysis*, J. C. Jansen, M. Stocker, H. G. Karge, J. Weitkamp, Eds. (Elsevier, New York, 1994), vol. 85, pp. 75–113.
- A. M. Chippindale and A. R. Cowley, *Zeolites* **18**, 176 (1997).
- X. Bu, T. E. Gier, P. Feng, G. D. Stucky, *Microporous Mater.*, in press.
- R. D. Shannon, *Acta Crystallogr. A* **32**, 751 (1976).
- L. B. McCusker, G. O. Brunner, A. F. Oju, *ibid.* **46**, C55 (1990); K. J. Andries and J. V. Smith, in preparation.
- Synthesis procedures and analytical data are available at <http://www.sciencemag.org/feature/data/974117.shl>. We thank Q. Huo for helpful discussions and D. Pierce from the Department of Geological Sciences for help with the electron probe microanalysis. This work was supported in part by the National Science Foundation under grant DMR 95-20971 and the U.S. Army Research Office under grant DAAH04-96-1-0443. A Materials Research Laboratory Corning Foundation Fellowship for P.F. is gratefully acknowledged.

14 August 1997; accepted 7 November 1997

Immune Versus Natural Selection: Antibody Aldolases with Enzymic Rates But Broader Scope

Carlos F. Barbas III,* Andreas Heine, Guofu Zhong, Torsten Hoffmann, Svetlana Gramatikova, Robert Björnstedt, Benjamin List, James Anderson, Enrico A. Stura, Ian A. Wilson,* Richard A. Lerner*

Structural and mechanistic studies show that when the selection criteria of the immune system are changed, catalytic antibodies that have the efficiency of natural enzymes evolve, but the catalytic antibodies are much more accepting of a wide range of substrates. The catalytic antibodies were prepared by reactive immunization, a process whereby the selection criteria of the immune system are changed from simple binding to chemical reactivity. This process yielded aldolase catalytic antibodies that approximated the rate acceleration of the natural enzyme used in glycolysis. Unlike the natural enzyme, however, the antibody aldolases catalyzed a variety of aldol reactions and decarboxylations. The crystal structure of one of these antibodies identified the reactive lysine residue that was selected in the immunization process. This lysine is deeply buried in a hydrophobic pocket at the base of the binding site, thereby accounting for its perturbed pK_a .

The central dilemma in the development of alternative protein catalysts concerns duplicating the rate accelerations of natural enzymes while increasing their versatility. For new enzymes to be optimally useful in chemistry, they must be both efficient and capable of accepting various substrates.

The authors are at The Skaggs Institute for Chemical Biology and the Department of Molecular Biology, The Scripps Research Institute, 10550 North Torrey Pines Road, La Jolla, CA 92037, USA.

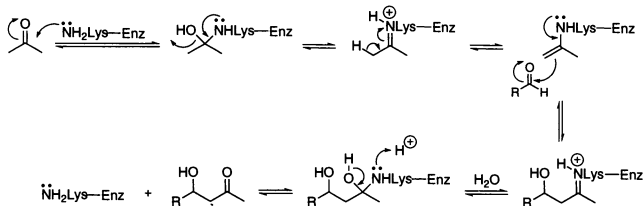
*To whom correspondence should be addressed.

Whereas the need for efficiency is obvious, the scope problem arises because enzymes would be more useful if they could catalyze a class of reactions with diverse substrates. To solve this problem, we have used antibody catalysis.

The approach is best highlighted by comparing the processes by which evolution and the immune system develop new protein functions. During evolution natural selection occurs as a consequence of improved function or fitness. In the case of

enzymes, selection is presumably based on catalytic efficiency where some enzymes reach "perfection" (1) through binding interactions being funneled into a chemistry that is most compatible with substrate turnover. By contrast, in the immune system, effective clonal selection is based on improved binding. Thus, whereas each system

taken to use antigens that are as inert as possible so that the resultant antibodies can interact with targets that are in their native state. In the process of reactive immunization, the opposite is done. A reactive antigen is designed so that a chemical reaction or reactions, such as the formation of a covalent bond, occurs in



Scheme 1.

has comparable genetic maneuvers to generate new functions, each differs in the selection criteria and time required (2). The central question is whether the immune system can yield efficient catalysts in real time if its selection criteria are switched from simple binding to function.

Our procedure, termed reactive immunization, allows for the production of antibodies with these desired properties (3, 4). The method provides a means to select antibody catalysts in vivo on the basis of their ability to carry out a chemical reaction. This procedure departs from the usual mode of immunization in which care is

taken to use antigens that are as inert as possible so that the resultant antibodies can interact with targets that are in their native state. In the process of reactive immunization, the opposite is done. A reactive antigen is designed so that a chemical reaction or reactions, such as the formation of a covalent bond, occurs in

the binding pocket of the antibody during its induction. The chemical reactivity programmed into the antibody is designed to be an integral part of a reaction coordinate when the corresponding substrates are used. The scope problem is also solved by reactive immunization because when the covalent event appears early in the process of evolution, further refinement of the binding pocket ceases.

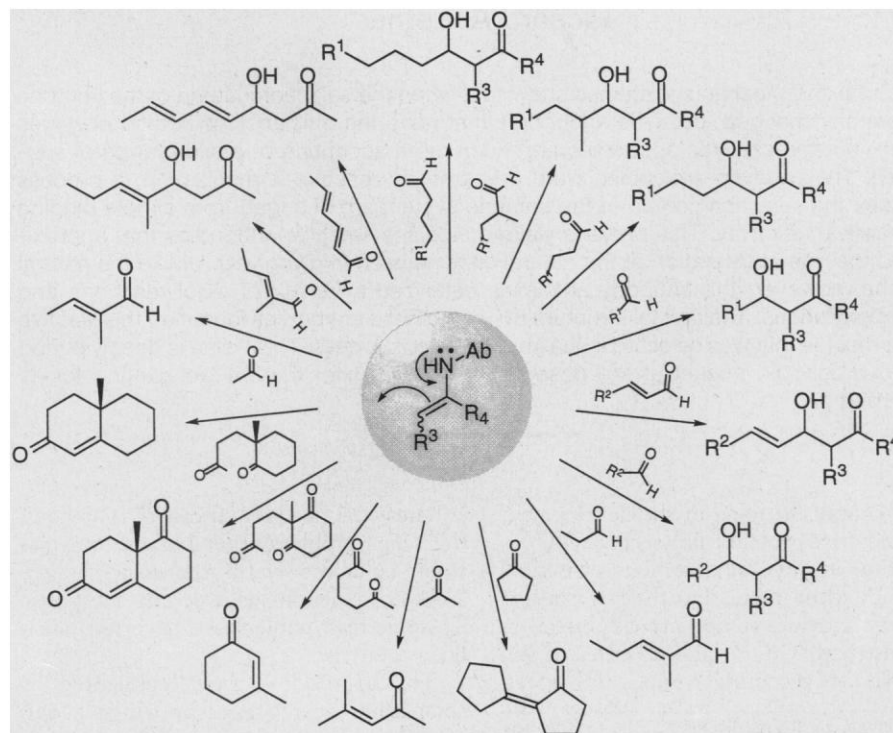
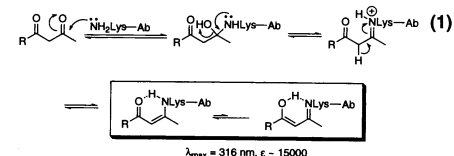


Fig. 1. Different ketones or aldehydes were used as substrates, and more than 100 aldehyde-aldehyde, aldehyde-ketone, and ketone-ketone aldol addition or condensation reactions have been catalyzed. R_1 , 4-acetamidobenzyl; R_2 , 4-nitrobenzyl; and R_3 and R_4 depend on the donor.

The reactive immunization process and the antibody aldolase. The antibody catalyst is an aldolase in which the enamine mechanism of the natural enzymes has been imprinted within the antibody binding site. Antibody 33F12 was prepared by immunizing mice with a 1,3-diketone hapten such that any antibody that had an appropriately placed lysine residue of the proper chemical reactivity would attack one of the hapten carbonyl groups to form a carbinolamine that would subsequently collapse to a Schiff base. A stable covalent interaction with the antibody is formed when the Schiff base tautomerizes to an enamine that, because of a second carbonyl functionality in the β position, is a stable vinylogous amide (Eq. 1).

The vinylogous amide has a strong ultraviolet absorption outside the range of the protein (approximately 316 nm) and, thus, instead of screening for binding, we screen for the new absorption that indicates that the antibody has evolved the central chemical mechanism of the natural aldolases. Antibodies made by this procedure have been shown to catalyze aldol (3, 5) and decarboxylation reactions (6), all of which proceed by the same enamine mechanism (7, 8) utilized by the natural class I aldolases. We now describe their scope, relative efficiency, and structure.

The enzyme fructose 1,6-diphosphate (FDP) aldolase is the most studied of the protein aldolases and is found in each of the three domains of life (7). The enzyme is central to glucose metabolism (glycolysis, sugar splitting, aldolase), catalyzing either net cleavage or synthesis during glycolysis



or gluconeogenesis, respectively. In nature, the enzyme catalyzes the cleavage of FDP to dihydroxyacetone phosphate and glyceraldehyde 3-phosphate. Class I aldolase enzymes proceed by the enamine mechanism (8) (Scheme 1). The mechanistic symmetry about the C-C bond-forming step allows the β -diketone selection to direct mechanistically identical reaction coordinates around this step (Eq. 1).

The scope and efficiency of the antibody catalyst. Unlike FDP aldolase, which is highly restricted, particularly with respect to donor activation (9), the antibody aldolase is very broad in scope, accepting a wide variety of substrates (Fig. 1). More than 100 different aldol additions or condensations, or both, have been effected by this single catalyst (Fig. 1). The catalyst is

capable of accelerating aldehyde-aldehyde, ketone-aldehyde, and ketone-ketone reactions. For cross-aldol reactions, various ketones are accepted as donors, such as aliphatic open chain (for example, acetone to pentanone series), aliphatic cyclic (cyclopentanone to cycloheptanone), functionalized open chain (hydroxyacetone, dihydroxyacetone, fluoroacetone), and functionalized cyclic (2-hydroxycyclohexanone) ketones. The active site lysine residue of the biocatalyst is able to convert these ketones into the corresponding enamines, which are key intermediates that are able to attack both aldehydes and ketones. As with the donors, the antibody also accepts different kinds of aldehyde substrates, such as pentanal, 4-acetamidobenzaldehyde, or 2,4-hexadienal. The antibody can also catalyze self-aldol condensations of acetone or cyclopentanone provided that no acceptor aldehyde is present for a cross-aldol reaction. In particular, propionaldehyde is also a substrate for a self-aldol condensation by acting as both a donor and acceptor. The reaction terminates at the dimer step although the product (*trans*-2-methyl-2-pentenal) contains a reactive aldehyde functionality and might be an acceptor itself for a subsequent addition step. Such a reaction is indeed catalyzed by the antibody but only when acetone was the donor. Here, no water elimination has occurred although the aldol addition product is labile to dehydration.

To determine whether water elimination, in the case of the self-aldol condensation reactions, was also catalyzed, we chemically synthesized the aldol addition product of cyclopentanone and incubated it with the antibody. Elimination of water from this substrate was catalyzed and followed typical Michaelis-Menten kinetics. In the case of intramolecular self-aldol condensations, the antibody catalyzed the formation of 3-methyl-2-cyclohexenone in one step with 2,6-heptanedione as substrate. This Baldwin-favored process (9a) is still catalyzed by the antibody if the 2,6-diketone is incorporated into a cyclohexanone system. Thus, the formation of A-B ring partial structures of steroids is catalyzed starting from the corresponding precursors. Most striking is the example in which the antibody catalyzes the cyclization of an achiral triketone to the (*S*)-enantiomer of the Wieland-Miescher ketone (first entry in Table 1) with an enantiomeric excess (*ee*) > 95% (5). These studies illustrate the power of reactive immunization, since the biocatalyst was not originally designed for acceptance of such a range of substrate geometries but rather for function (3).

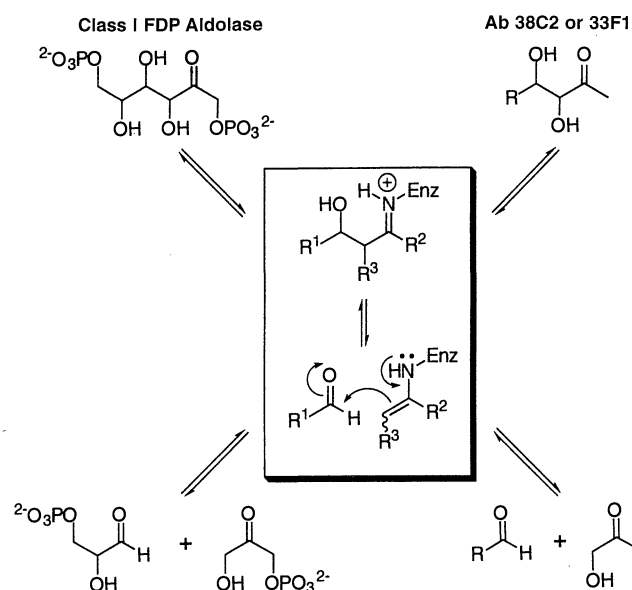
All the antibody-catalyzed aldol reactions followed typical Michaelis-Menten kinetics except for the benzaldehyde deriva-

tives that gave a slight substrate inhibition at higher concentrations (>2 mM) (9b). Typical values for the Michaelis constants K_m of the donors in cross-aldol reactions ranged from 1 mM to 1 M, reflecting the ability of the antibody to accept various different ketones. Values for K_m of the acceptor aldehydes ranged from 20 μ M to 500 μ M. The aromatic portion of these

molecules is in part responsible for an increased recognition by the active site. In addition, the hydrophobicity of these compounds facilitates their partitioning into the active site. In self-aldol and intramolecular aldol condensation reactions, values for K_m range from 1 to 5 mM. The K_m 's for the retroaldol reactions were lower and typically ranged from 15 to 400

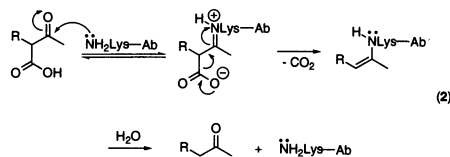
Table 1. Kinetic parameters for a selection of antibody-catalyzed aldol and *retro*-aldol reactions, reflecting the ability of the biocatalyst to accept substrates that clearly differ with respect to their geometry. No background reaction was observed for the cyclopentanone self-condensation. The value for the addition of cyclopentanone to pentanal was estimated using $k_{\text{uncat}} = 2.28 \cdot 10^{-7} \text{ M}^{-1} \text{ min}^{-1}$ for the aldol addition of acetone to an aldehyde from (34).

Substrate	Product	k_{cat} (min^{-1})	$k_{\text{cat}}/k_{\text{uncat}}$
		0.086	$3.6 \cdot 10^6$
		$3 \cdot 10^{-4}$	nd
		1.02	$4.5 \cdot 10^6$
		2.14	nd
		5.0	nd



μM . Characteristic values for k_{cat} of all reactions ranged from 10^{-3} to 5 min^{-1} with a ratio of $k_{\text{cat}}/k_{\text{uncat}}$ of 10^5 to 10^7 .

In that both the natural enzyme and the antibody can catalyze the cleavage of a β -hydroxy ketone to an aldehyde and a ketone, we compared the efficient cases for each that are highly similar *retro*-aldol reactions (Fig. 2). For FDP aldolase, the preferred reaction is the cleavage of FDP to dihydroxyacetone phosphate and glyceraldehyde 3-phosphate. In the antibody case, the cleavage of 6-(4'-dimethylaminophenyl)-4-hydroxy-5-hexen-2-one to acetone and 4-dimethylamino-cinnamaldehyde is preferred. The antibody avoids the need for the charged phosphate moiety on the natural substrate. The catalytic turnover achieved by the antibodies is within 10 times that of the natural enzyme (about 1/s) for the optimal substrates of each (7, 8). Further, the turnover efficiency of the antibody is maintained for a variety of reactions (Table 1).



Dependence of the evolution of diverse catalytic function on initial reactivity. In addition to the aldol reaction, the antibody catalyzes the decarboxylation of β -keto acids with a protonated Schiff base serving as the electron sink (Eq. 2) (6). Indeed, a few natural aldolases have been shown to catalyze biologically relevant decarboxylation reactions in a mechanistically analogous fashion (10). An alternative route to diversification of mechanism involves the use of cofactors. In natural enzymes, cofactors expand the repertoire of reactions catalyzed. If a catalyst, such as antibody 33F12, is envisioned as a model of a primordial catalyst, its scope could be expanded by the presence of a cofactor, such as pyridoxal phosphate, with subsequent evolutionary refinement. This relatively simple maneuver would convert an enzyme with an active site lysine into a pyridoxal-dependent enzyme capable of catalyzing many amino acid-based transformations. These reactions include transaminations, racemizations, decarboxylations, aldol reactions, and elimination and replacement reactions (11). In these enzymes, the coenzyme is bound in a reversible iminium linkage formed by a reaction between the ϵ -amino group of the active site lysine and the carbonyl group of the cofactor to form an imine that has a characteristic absorption between 360 and 420 nm. To test these ideas, we studied the ability of the catalytic antibody to sequester the cofactor pyridoxal

in its active site, and found that the antibody 33F12 binds the cofactor in the typical internal aldimine fashion (Fig. 3). Subsequent addition of 2,4-pentanedione showed that the aldimine was formed reversibly with the same lysine residue used in the aldol chemistry. The same activity was observed with another antibody 38C2. This simple addition of a natural cofactor may extend the scope of the aldolase antibodies and, thereby, allow a diverse new class of reactions. In this way, we might duplicate experimentally a process that nature has used to create enzyme diversity from initial reactivity (11).

A chemically reactive lysine. In that the rate accelerations of the two aldolases are comparable, we examined the ways that clonal selection and natural selection each resolved the chemical problems in the catalytic event. The first step in the aldol reaction is the nucleophilic attack of an ϵ -amino group of lysine on a carbonyl group. For the ϵ -amino group to be nucleophilic, it must be in its uncharged form. However, the pK_a of the amino group of lysine in aqueous solution is 10.5 (12). Because both natural and antibody aldolases depend on a nonprotonated lysine as a nucleophile and operate with maximal activity at neutral pH where the ϵ -amino group of lysine normally would be

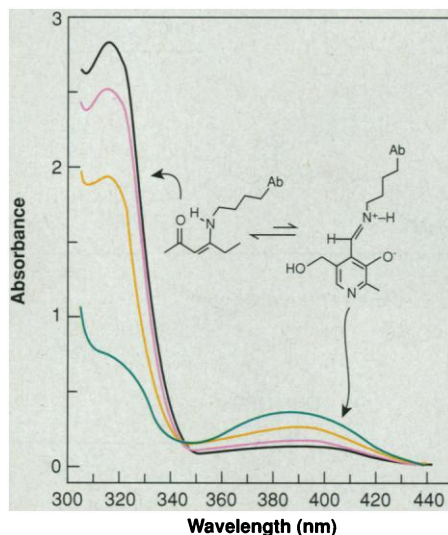
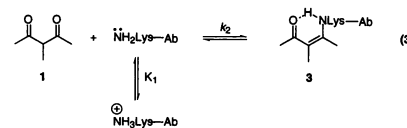


Fig. 3. Antibody 33F12 binds pyridoxal via a reversible imine linkage. Incubation of $30 \mu\text{M}$ antibody and $120 \mu\text{M}$ pyridoxal at pH 7.4 results in a broad absorption with a maximum at 390 nm resulting from the formation of an internal aldimine. Subsequent addition of $100 \mu\text{M}$ 2,4-pentanedione produced a time-dependent decay of this absorption and with the appearance of a new absorption maxima corresponding to the enamine at 316 nm . Spectra were collected after incubation of antibody and cofactor at 25°C for 1 min (green); and after addition of 2,4-pentanedione for 1 min (black), 3 min (blue), and 5 min (red curve).

protonated, the pK_a of this group must be perturbed.

The dependence of k_{cat}/K_m and $1/K_m$ as a function of pH for the retroaldol reaction



shows an acidic limb $\text{pK}_a = 6.3$ to 6.6 and approximates the pH dependence of catalysis of FDP aldolase (8). Ideally, the dependence of k_{cat}/K_m and $1/K_m$ on pH should follow the ionization state of the free catalyst and free substrate. However, in a complex mechanism with several intermediates at different degrees of protonation, a kinetically determined pK_a may not represent a real ionization constant, in that it can be composed of ratios of several rate constants and the rate-limiting step may change with pH. A more straightforward approach to determine the pK_a of the essential lysine, one that avoids some of the complexity of the retro-aldol reaction, is based on the ability of the antibodies to form enamines with β -diketones. The aldol antibodies react stoichiometrically with β -diketones, such as 3-methyl-2,4-pentanedione, to form stable vinylogous amides (Eq. 3) that completely inhibit aldolase activity. The reaction of 3-methyl-2,4-pentanedione was monitored spectrophotometrically by following the absorption of the antibody-enamine complex 3 now at 335 nm . The pH dependence of this reaction is described by a titration curve with a pK_a of 5.5 and 6.0, for antibodies 33F12 (Fig. 4) and 38C2, respectively (13). Study of the dependence of the rate of enamine formation on pH with 2,4-pentanedione yielded the same

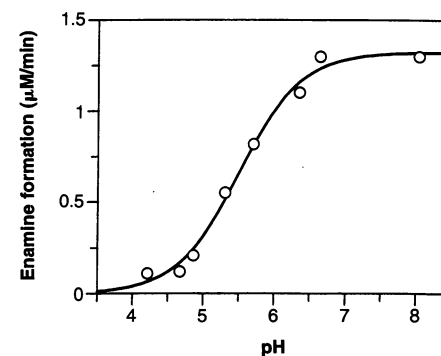


Fig. 4. Rate of enamine formation as a function of pH. Enamine formation between antibody 33F12 and 3-methyl-2,4-pentanedione was followed spectrophotometrically at 335 nm , at 15°C . The incubation mixtures contained $7.5 \mu\text{M}$ antibody and $250 \mu\text{M}$ 3-methyl-2,4-pentanedione in citrate-phosphate buffer in the pH range from 4.2 to 8. The reaction velocities were calculated with the use of the experimentally determined extinction coefficient $\epsilon_{335} = 9.1 \text{ mM}^{-1}\text{cm}^{-1}$.

pK_a . The pK_a 's of the protons at the 3 positions of 2,4-pentanedione and 3-methyl-2,4-pentanedione are 8.87 and 10.65, respectively (14). These studies, together with those of the pH dependence of retroaldol activity, demonstrate that these proteins contain active-site lysines with perturbed pK_a 's. From the work of Westheimer and his colleagues on another Schiff base-forming enzyme, acetoacetate decarboxylase, we know that chemical tuning of a reactive lysine for Schiff base formation at neutral pH may be accomplished, at least in part, by proximity of a neighboring protonated lysine residue that electrostatically perturbs the pK_a of the amine nucleophile (13, 15). An alternative mechanism for the perturbation of the pK_a of an amine is based on a hydrophobic microenvironment (16).

A promiscuous hydrophobic pocket surrounding a structurally unusual lysine. In order to gain a better structural understanding of the nucleophilic character of the single reactive Lys within these antibodies (3) and to explore the structural features that explain their scope, we cloned and sequenced their genes and then determined the three-dimensional x-ray crystal structure of the Fab' antigen binding fragment of antibody 33F12. The sequences of 33F12 and 38C2 revealed 26 and 25 Lys residues, respectively. The antibodies were found to be somatic variants of a single VDJ rearrangement and differed by nine amino acids each in V_L and V_H .

The structure of Fab'33F12 was determined by molecular replacement at 2.15 Å resolution (Table 2). The overall structure of the native Fab is similar to other known

Fab structures (Fig. 5, A and B). The elbow angle, which relates the pseudo-twofold axes of the V_L - V_H and C_L - C_H1 to each

Table 2. Data collection and refinement statistics. The Fab' of the aldolase antibody 33F12 crystallizes from 18% PEG 4000, 0.1 M Hepes, pH 7.4, and 10% isopropanol. A native data set was collected at SSRL, beamline 7-1, at -176°C with 25% glycerol as a cryoprotectant. Data were processed with DENZO and SCALEPACK (17). The structure was determined by molecular replacement techniques. From 86 initial search models, antibody NC6.8 (18) gave a rotation function solution with MERLOT (17) of 7.6σ in the resolution range 10 to 4 Å. A rotational and translational search using data from 15 to 4 Å in the program AMORE (17) gave an $R = 44.7\%$ with a correlation coefficient of 49.6, compared to the next, incorrect solution of $R = 55.6\%$ and a correlation coefficient of 19.4. Computational mutation to the correct sequence and multiple rounds of model building were done with the program O (17). The initial refinement in X-PLOR (17), with rigid body, positional and slow-cooling refinement protocols, resulted in an $R = 23.8\%$ for 10.0 to 2.15 Å data with $F > 1\sigma_F$. Refinement was then continued with SHELXL-96 (17). For each refinement step, at least 10 cycles of conjugate gradient minimization with individual B value refinement were performed, with restraints on bond distances, angles, and B factors. In the final stages, hydrogen atoms were placed in calculated positions without use of additional parameters. The overall map quality was good, showing no main chain breaks except for a region H128-H136 in the constant heavy chain, as frequently observed in other antibodies (19). The only outlier in the Ramachandran plot is residue Val^{L51}, as commonly observed in other Fabs (20). The density for Lys^{H93} is bulky at a 2σ level and does not extend beyond C_ϵ (21), possibly indicating multiple side chain conformations, as frequently observed for Lys residues in proteins (22).

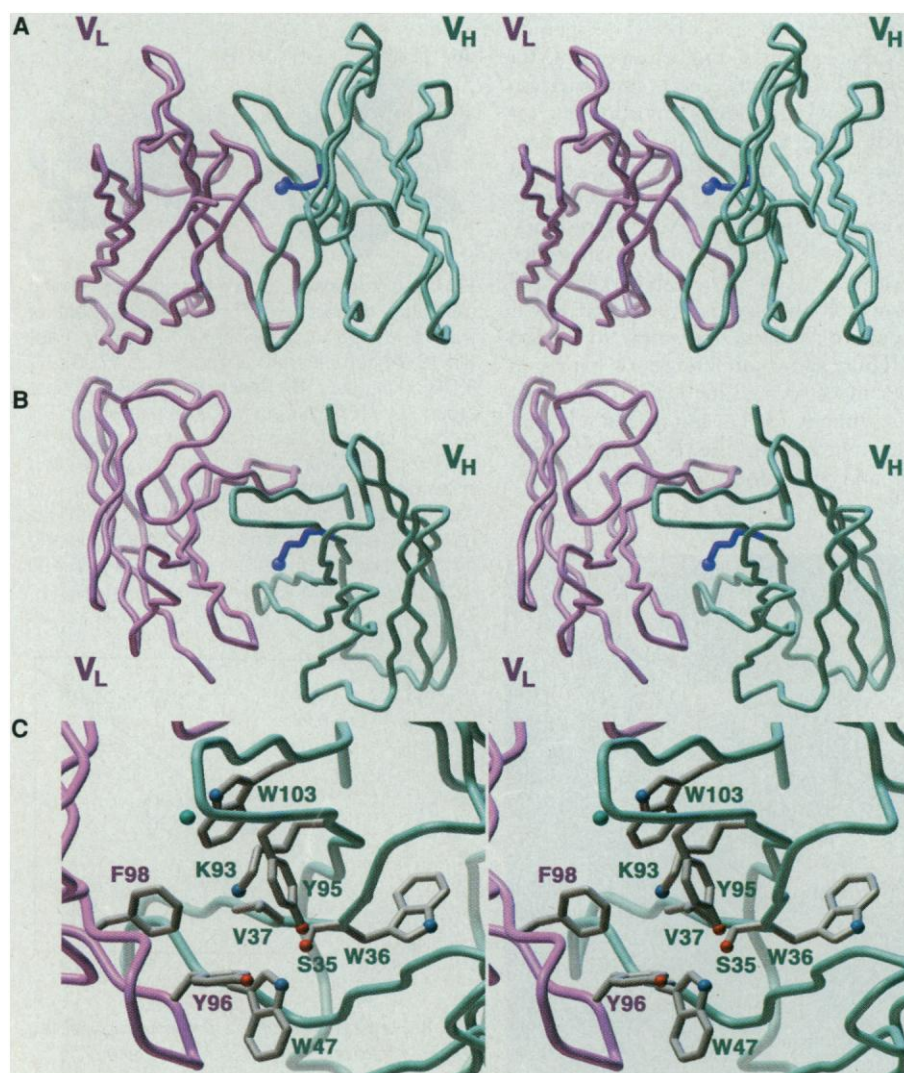


Fig. 5. Stereoview of the Fab' variable region (V_H , V_L) of antibody 33F12. (A) The side view shows the position of Lys^{H93} at the bottom of hypervariable loop H3. (B) Rotation by 90° shows the corresponding top view, looking directly into the binding site. (C) Stereoview of the Fab' 33F12 binding site, showing only side chains for residues (<4 Å) within the vicinity of Lys^{H93}. The light chain is colored in pink and the heavy chain in blue with the side chains of the neighboring residues labeled.

Space group	$P2_12_12_1$
Unit cell dimensions	$a = 56.5$ Å $b = 65.3$ Å $c = 132.6$ Å
Resolution range (Å)	40 to 2.15
Observations (N)	264,288
Unique reflections (N)	26,432
Completeness (%)	96 (95)*
(I/σ_I)	25.3 (5.6)*
R_{merge} (%)	6.5 (30.2)*
Refined residues	434
Refined water molecules	248
Resolution range in refinement (Å)	10.0 to 2.15
R_{cryst} (%), ($24776 F_o$; $21174 F_o > 4\sigma F_o$)	21.1; 19.3
R_{free} (%), ($1304 F_o$; $1127 F_o > 4\sigma F_o$)	31.7; 29.1
Deviations from ideal geometry (rms)	
Bond lengths (Å)	0.006
Bond angles ($^\circ$)	1.8
Dihedral angles ($^\circ$)	30
Improper angles ($^\circ$)	1.7
Ramachandran plot (%)	90.2; 9.5; 0; 0.3†
B factor	
Average protein (Å^2)	29
Waters (Å^2)	37

*Outer shell 2.23 to 2.15 Å. †Order: most favored, additional allowed, generously allowed, and disallowed regions, from Procheck (17).

other is 151.4° and within the observed range for Fab molecules (23). The entrance of the antigen binding site of 33F12 is a narrow elongated cleft (Fig. 6). The binding pocket is more than 11 Å deep, expanding with depth (24) and is comparable to combining sites of antibodies raised against other small haptenic molecules (25). At the bottom of the pocket, Lys^{H93} is found within a hydrophobic environment (Fig. 5C). A second Lys^{H52b} is located at the top of CDR-H2, with its side chain pointing toward the outside of the molecule. In antibody 38C2, Lys^{H52b} is mutated to an Arg while Lys^{H93} is common to both. A sequence comparison of the CDRs with other known antibody molecules reveals some unusual features of antibody 33F12. Residue H93 is Ala in most antibodies (26). Only two other antibodies of known structure contain a Lys in that position: the esterolytic antibody 17E8 (27) and the chimeric Fab fragment of the carcinoma-binding antibody B72.3 (28). Furthermore, residue H94, which is usually an Arg in other antibodies, is replaced by a hydrophobic Ile in 33F12. The Arg at position H94 frequently forms a salt bridge with an aspartic acid at H101. Utilization of the JH3 germline by both antibodies, the only JH segment not to encode an Asp at this position, precludes this commonly observed interaction.

Analysis of the combining site of Fab' 33F12 (Fig. 7A) shows that Lys^{H93} is surrounded by mostly hydrophobic side chains and is in van der Waals contact with residues Leu^{H4}, Met^{H34}, Val^{H37}, Cys^{H92}, Ile^{H94}, Tyr^{H95}, Ser^{H100}, Tyr^{H102}, and Trp^{H103}.

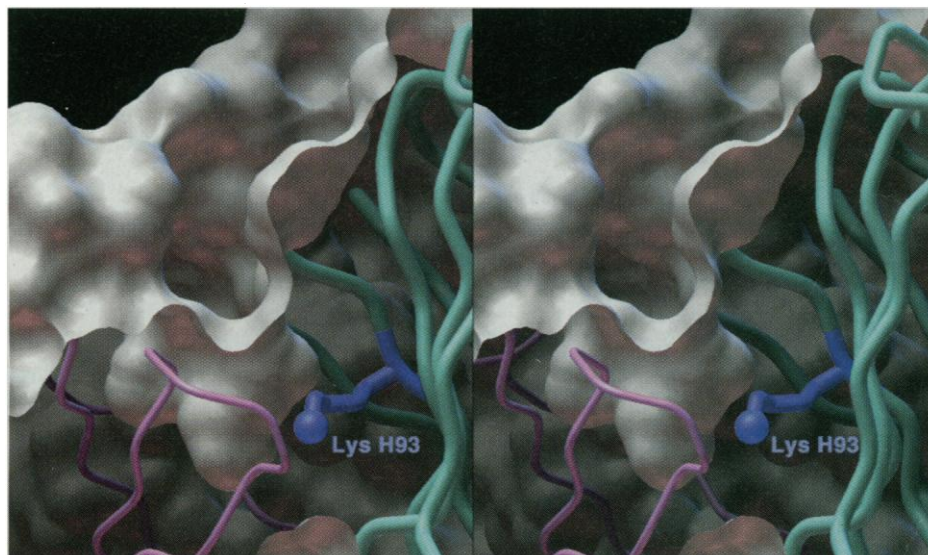


Fig. 6. Stereoview of the 33F12 Fab' binding pocket. A slice is shown through the molecular surface calculated with a 1.4 Å sphere radius. Only the amino tip of residue Lys^{H93}N ζ is in contact with the molecular surface at the bottom of the antigen-combining site. The light chain is shown in pink, the heavy chain in blue.

With the exception of Ile^{H94}, which is a Thr in 38C2, the residues in van der Waals contact with Lys^{H93} are conserved in both antibodies. Further, all other residues are encoded in the germline gene segments used by these antibodies. The V gene-encoded residues that differ between the antibodies contribute little to the refinement of the binding pocket, suggesting that Lys^{H93} appeared early in the ontogeny of these catalysts and the remaining mutations were the result of neutral drift during immunological selection. Within this pocket, only one charged residue is within an 8 Å radius of the N ζ of Lys^{H93}. The carboxyl of Glu^{H50} is located at about 7.4 Å, too far for formation of any hydrogen bond or salt bridge. In addition, Lys^{H93} does not form any hydrogen bonds with any main chain carbonyl oxygens.

In antibody B72.3, Asp^{H101} is absent, but Lys^{H93} forms a charged hydrogen bond with the main chain carbonyl oxygen of Tyr^{H96} that is proposed to be responsible for its unusual CDR-H3 loop conformation (28). The corresponding environment for antibody 17E8 is shown in Fig. 7B. Also described is a hydrophobic pocket for substrate recognition (27), in addition to the charged Arg^{H94} and Asp^{H101} residues. Here, the Lys^{H93} residue forms a salt bridge to Asp^{H101} (Lys^{H93}N ζ -Asp^{H101}O δ 1 3.2 Å) in which the positively charged Lys is proposed to stabilize oxyanion formation (27). Thus, as no salt bridges or hydrogen bonds can be formed for Lys^{H93} in our aldolase antibody 33F12, and it is in a hydrophobic environment, the pK_a would be perturbed and allow the uncharged Lys^{H93} to

function as a strong nucleophile.

In order to define further the mechanism by which the pK_a of the ϵ -amino group was perturbed, we synthesized a series of related β -hydroxy ketone substrates that differed in a defined manner with respect to their hydrophobicity. A study of the linear free energy relation between substrate partitioning into *n*-octanol and k_{cat}/K_m , the Hansch correlation (29), shows that the active site of antibody 33F12 is 1.1 times more hydrophobic than *n*-octanol (Fig. 8). This analysis, together with the observation that the antibody lacks a positively charged amino acid side chain in the vicinity of Lys^{H93}, supports the possibility that the pK_a of Lys^{H93} is perturbed by a hydrophobic microenvironment that disfavors protonation and charge development on its ϵ -amino group in the unliganded antibody.

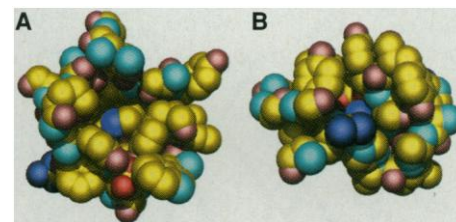


Fig. 7. Comparison of two antibody-combining sites that contain Lys^{H93}. The environment of Lys^{H93} is very hydrophobic in antibody Fab' 33F12 (A) compared to antibody Fab 17E8 (27) (PDB code 1eap) (B). Residues in an 8 Å sphere around Lys^{H93}N ζ are shown. A space-filling CPK representation of the environment around Lys^{H93} is shown with hydrophobic atoms in yellow, and polar nitrogen and oxygen atoms in cyan and salmon, respectively. Charged basic residues have their nitrogen atoms colored dark blue and charged oxygen atoms are colored in red. The Lys^{H93}N ζ atom is colored in blue.

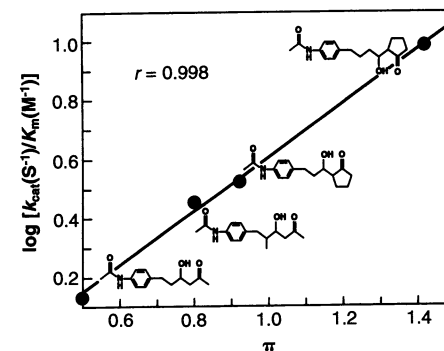


Fig. 8. Hansch plot for the determination of the relative hydrophobicity of the active site. The kinetic constants (k_{cat}/K_m) for antibody 33F12-catalyzed *retro*-aldol reaction of a series of aldols, R¹CH(OH)CHR²C(O)R³, were plotted as a function of the hydrophobicity constant π of the corresponding R substituents. The π values were calculated as described (29).

We thus have a picture of the evolutionary events that lead to the efficiency and promiscuity of this catalyst. A lysine residue appeared early during somatic refinement in a germ line antibody containing an otherwise hydrophobic pocket. The insertion of this residue into this hydrophobic microenvironment resulted in chemical reactivity that was efficient enough to be selectable. Once this covalent process appeared, the binding pocket did not further evolve toward high specificity.

A vantage point on enzyme evolution. Protein enzymes achieve their efficiency, in part, as a result of transition-state stabilization, strain, acid-base catalysis, and proximity (1, 30, 31). The protein scaffold of each enzyme has evolved to permit the concerted interaction of these individual effects so that together they provide remarkable rate accelerations (31). The requirement for these concerted effects, as facilitated by a permissive protein scaffold, has led to questioning whether artificial proteins can match the efficiency of natural enzymes.

In principle, the catalytic potential of proteins can be explored by antibodies because a set of binding pockets can be programmed to interact with substrates much as enzymes do. Although many catalytic antibodies have been made and shown to have good rate accelerations (2), it has not been possible to compare them to natural enzymes because they use different mechanisms. Thus, the fundamental question about whether other proteins can be made as efficient as natural enzymes had not been answered. We now show that antibodies and enzymes can be of comparable catalytic efficiency when each uses a similar mechanism.

We do not suggest that catalytic antibodies will prove to be as efficient as all enzymes. However, a catalytic antibody can approximate the turnover efficiency of a highly evolved natural enzyme that is central to energy metabolism in all living organisms. Fructose 1,6-diphosphate aldolase could be considered a special case in that a single amino acid plays such a key role in the catalytic mechanism. But, this apparent simplicity is deceptive in that the chemical nature of that amino acid must be tuned by its local environment. Structural and chemical studies of our catalytic antibodies suggest that the pK_a of the key ϵ -amino group of Lys^{H93} is lowered by its hydrophobic environment, which disfavors protonation and development of charge on the amino functionality. Selection of an antibody requires an active site lysine that is sufficiently nucleophilic to attack the carbonyl carbon and form a stable vinylogous amide. Furthermore, the dynamics of water, key in this reaction and for the aldol, are also

programmed into this selection.

We have catalyzed more than 100 aldehyde-aldehyde, aldehyde-ketone, and ketone-ketone aldol addition or condensation reactions. Some of these reactions, such as the construction of the Wieland-Miescher ketone, are central to the theory and practice of organic chemistry. They have played a role in the synthesis of structures as diverse as steroids and taxol. The broad substrate specificity of the antibody aldolases is a property shared by other catalytic antibodies prepared by reactive immunization (4) and, as discussed above, is likely to be the result of the special ontogeny of antibodies induced by immunogens that form covalent bonds within the binding pocket during induction. This situation is in contrast to what is observed in immunological selections based on transition-state analogs that result in highly complementary binding pockets of limited scope (32). Our x-ray crystallographic and biochemical studies support the contention that the antibody contains a promiscuous binding pocket with a lysine located in a hydrophobic environment at its base. The binding pocket is expected to accommodate various substrates that are drawn into the pocket as a result of hydrophobic partitioning. Once in the binding pocket, the substrates encounter the highly reactive lysine nucleophile and collapse to the nucleophilic enamine. Likewise, the aldol acceptor can enter the pocket and, so long as there are no prohibitive steric interactions, participates in an aldol addition. The large number of different reactions that the antibody aldolases catalyze is compatible with this scheme.

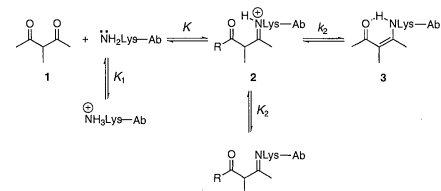
Finally, because the aldolase catalytic antibodies are in many ways analogous to complex enzymes, we may learn something about the evolution of metabolic enzymes. The answer to the question of how difficult it is to achieve complex catalytic function is key in furthering our notions of the origin of life. The process of reactive immunization switches the usual evolutionary cycle of variation and selection to one in which, for the most part, selection precedes variation. Our experiments imply that it is apparently relatively simple to move from binding of reactive materials to a complex catalytic function that is efficient enough to be selectable. Once natural selection begins to optimize that function, the protein becomes refined, not only in carrying out the relevant chemical reaction but also in adapting its activity to a more complicated metabolic scheme, such as glucose metabolism. Ultimately, the process of adaptation would refine the scope of catalysis to a narrow context in which context-specific

regulatory processes would operate. But prior to that narrowing, an enzyme of broad specificity could serve as the starting point for the evolution of a family of related enzymes. With the vantage point that the evolution of an efficient chemical mechanism is a primary driving force in enzyme evolution and a starting point for diversification of function, it is anticipated, as well as observed, that structurally different proteins may converge on an efficient and identical chemical mechanism based on their ability to adapt their active sites (33).

It may be that an early defining event in the evolution of some enzymes was an interaction with reactive materials, such as toxins, in a process similar to the induction of these catalytic antibodies with a reactive immunogen. The chemical reactivity of the primordial stoichiometric protein could then serve as a template for the rapid evolution of diverse catalytic function. This would be facilitated by gene duplication events, allowing each enzyme copy to be free to diversify and become specifically optimized for a particular substrate. In terms of the many reactions described here, each one could be selectively optimized after a gene duplication event.

REFERENCES AND NOTES

- W. J. Albery and J. R. Knowles, *Angew. Chem. Int. Ed., Engl.* **16**, 285 (1977).
- P. G. Schultz and R. A. Lerner, *Science* **269**, 1835 (1995).
- J. Wagner, R. A. Lerner, C. F. Barbas III, *Science* **270**, 1797 (1995).
- P. Wirsching, J. A. Ashley, C.-H. Lo, K. D. Janda, R. A. Lerner, *ibid.*, p. 1775.
- G. Zhong, T. Hoffmann, R. A. Lerner, S. Danishefsky, C. F. Barbas III, *J. Am. Chem. Soc.* **119**, 8131 (1997).
- R. Björnstedt, G. Zhong, R. A. Lerner, C. F. Barbas III, *ibid.* **118**, 11720 (1996).
- J. J. Marsh and H. G. Leberz, *Trends Biochem. Sci.* **17**, 110 (1992); W. J. Rutter, *Fed. Proc. Am. Soc. Exp. Biol.* **23**, 1248 (1964).
- C. Y. Lai, N. Nakai, D. Chang, *Science* **183**, 1204 (1974); A. J. Morris and D. R. Tolan, *Biochemistry* **33**, 12291 (1994).
- C.-H. Wong, R. L. Halcomb, Y. Ichikawa, T. Kajimoto, *Angew. Chem. Int. Ed. Engl.* **34**, 412 (1995).
- J. E. Baldwin and M. J. Lusch, *Tetrahedron* **38**, 2939 (1982).
- 9b. ———, unpublished results.
- C. J. Vlahos and E. E. Decker, *J. Biol. Chem.* **261**, 11049 (1986).
- R. A. John, *Biochim. Biophys. Acta* **1248**, 81 (1995); H. Wada and E. E. Snell, *J. Biol. Chem.* **237**, 133 (1962).
- J. A. Dean, in *Lange's Handbook of Chemistry* (McGraw-Hill, San Francisco, 1992), pp. 8.19–8.71.
- Although the rate of enamine formation may be described by Eq. 3, the more complicated kinetic scheme



is better described by the equation:

$$\text{Rate}_{\text{obs}} = k_2[1]/(1+[H^+]/K_2)$$
$$\frac{K(1+[H^+]/K_1)}{(1+[H^+]/K_2)} \cdot [1]$$

This equation is simplified by choosing conditions wherein Michaelis-Menten kinetics are not followed and the reaction between antibody and diketone are second order. Under these conditions, the value for [1] in the denominator becomes negligible and the equation reduces to a description of a simple titration curve that reflects K_1 , that is, the ionization constant of the essential lysine:

$$\text{Rate}_{\text{obs}} = \frac{(k_2/K)[1]}{(1+[H^+]/K_1)}$$

These kinetic arguments follow from D. E. Schmidt Jr. and F. H. Westheimer [*Biochemistry* **10**, 1249 (1971)].

14. P. Y. Bruice, *J. Am. Chem. Soc.* **112**, 7361 (1990).
15. P. A. Frey, F. C. Kokesh, F. H. Westheimer, *ibid.* **93**, 7266 (1971); F. C. Kokesh and F. H. Westheimer, *ibid.*, p. 7270; L. A. Highbarger, J. A. Gerlt, G. L. Kenyon, *Biochemistry* **35**, 41 (1996).
16. J. K. Lee and K. N. Houk, *Science* **276**, 942 (1997); S. Daopin, D. E. Anderson, W. A. Baase, F. W. Dahlquist, B. W. Matthews, *Biochemistry* **30**, 11521 (1991).
17. X-ray crystallographic programs and methods: (i) HKL (DENZO and SCALEPACK); Z. Otwinowski and W. Minor, *Methods Enzymol.* **276**, 307 (1997); (ii) MERLOT; P. M. D. Fitzgerald, *J. Appl. Crystallogr.* **21**, 273 (1988); (iii) AMORE; J. Navaza, *Acta Crystallogr.* **A50**, 157 (1994); (iv) Program O; T. A. Jones, J.-Y. Zou, S. W. Cowan, M. Kjeldgaard, *ibid.* **A47**, 110 (1991); (v) X-PLOR; A. T. Brünger, J. Kuriyan, M. Karplus, *Science* **235**, 458 (1987); A. T. Brünger, X-PLOR, *Version 3.1: A System for X-ray and NMR* (Yale Univ. Press, New Haven, CT, 1992); (vi) SHELXL; G. M. Sheldrick, SHELXL-96, Program for crystal structure refinement, Göttingen, 1996 (VII). Procheck; R. A. Laskowski, M. W. MacArthur, S. D. Moss, J. M. Thornton, *J. Appl. Crystallogr.* **26**, 283 (1983).
18. L. W. Guddat, L. Shan, J. M. Anchin, D. S. Linthium, A. B. Edmondson, *J. Mol. Biol.* **236**, 247 (1994).
19. R. L. Stanfield, T. M. Fieser, R. A. Lerner, I. A. Wilson, *Science* **248**, 712 (1990).
20. J. A. Arevalo, E. A. Stura, M. J. Taussig, I. A. Wilson, *J. Mol. Biol.* **231**, 103 (1993).
21. At 1.5 σ , the density showed the complete residue; and density appeared close to the Lys^{H93}, which could not be refined as a water molecule and might be a cryoprotectant or precipitant molecule that is partially occupied. However, the density gave no clear indication at this resolution as to its identity.
22. J. S. Richardson and D. C. Richardson, in *Prediction of Protein Structure and The Principles of Protein Conformation*, G. D. Fasman, Ed. (Plenum, New York, 1990), p. 1.
23. I. A. Wilson and R. L. Stanfield, *Curr. Opin. Struct. Biol.* **4**, 857 (1994).
24. The depth of the binding pocket was estimated from measurement of the following: Lys^{H93}N ζ -Thr^{L92}C α 11.1 \AA , Lys^{H93}N ζ -His^{L93}C α 11.6 \AA , Lys^{H93}N ζ -Tyr^{H97}C α 12 \AA .
25. D. R. Davies, E. A. Padlan, S. Sheriff, *Annu. Rev. Biochem.* **59**, 439 (1990); L. C. Hsieh-Wilson, P. G. Schultz, R. C. Stevens, *Proc. Natl. Acad. Sci. U.S.A.* **93**, 5363 (1996).
26. E. A. Kabat et al., Eds, *Sequences of Proteins of Immunological Interest* (National Institutes of Health, Bethesda, MD, ed. 5, 1991).
27. G. W. Zhou, J. Guo, W. Huang, R. J. Fletterick, T. S. Scanlan, *Science* **265**, 1059 (1994).
28. R. L. Brady et al., *J. Mol. Biol.* **227**, 253 (1992).
29. J. Hine and F. A. Via, *J. Am. Chem. Soc.* **94**, 190 (1972); C. Hansch and E. Coats, *J. Pharmacol. Sci.* **59**, 731 (1970); J. Fastrez and A. R. Fersht, *Biochemistry* **12**, 1067 (1973); A. Leo, C. Hansch, D. Elkins, *Chem. Rev.* **71**, 525 (1971).
30. W. P. Jencks, in *Catalysis in Chemistry and Enzymology*, A. Meister, Ed. (Dover, Mineola, NY, 1975).
31. J. R. Knowles, *Nature* **350**, 121 (1991).

32. G. J. Wedemayer, P. A. Patten, L. H. Wang, P. G. Schultz, R. C. Stevens, *Science* **276**, 1665 (1997).
33. G. Hester et al., *FEBS Lett.* **292**, 237 (1991).
34. J. L. Reymond and Y. Chen, *J. Org. Chem.* **60**, 6970 (1995).
35. We thank W. Gilbert and A. Eschenmoser for helpful discussions; the Stanford Synchrotron Radiation Laboratory for data collection time; the staff of beamline 7-1 for their support; G. Fieser, R. Fuller, D. Kubitz, and R.

Stefanko for technical assistance; M. Pique for production of figures; and the Alexander von Humboldt Foundation, Germany, for a Feodor Lynen Fellowship (T.H.). Supported by NIH CA27489 (R.A.L., I.A.W., C.F.B.). Coordinates and structure factors for the Fab' 33F12 have been deposited with Brookhaven Data Bank, with PDB ID code 1axt for the coordinate entry.

14 July 1997; accepted 9 November 1997

Transcription Regulation by Initiating NTP Concentration: rRNA Synthesis in Bacteria

Tamas Gaal, Michael S. Bartlett, Wilma Ross, Charles L. Turnbough Jr., Richard L. Gourse*

The sequence of a promoter determines not only the efficiency with which it forms a complex with RNA polymerase, but also the concentration of nucleoside triphosphate (NTP) required for initiating transcription. *Escherichia coli* ribosomal RNA (*rrm* P1) promoters require high initiating NTP concentrations for efficient transcription because they form unusually short-lived complexes with RNA polymerase; high initiating NTP concentrations [adenosine or guanosine triphosphate (ATP or GTP), depending on the *rrm* P1 promoter] are needed to bind to and stabilize the open complex. ATP and GTP concentrations, and therefore *rrm* P1 promoter activity, increase with growth rate. Because ribosomal RNA transcription determines the rate of ribosome synthesis, the control of ribosomal RNA transcription by NTP concentration provides a molecular explanation for the growth rate-dependent control and homeostatic regulation of ribosome synthesis.

Protein synthesis is the dominant activity of the bacterial cell (1). Ribosome synthesis rates increase approximately with the square of the growth rate to increase protein synthesis at higher growth rates and to conserve biosynthetic energy at lower growth rates. The relation between growth rate and ribosome synthesis rate, referred to as growth rate-dependent control, was described almost 40 years ago and has been the subject of intensive investigation ever since (2, 3). Models have been proposed to explain the phenomenon, but the molecular mechanism or mechanisms responsible have not been determined (4).

Ribosomal RNA (rRNA) transcription is the rate-limiting step in ribosome synthesis, because ribosomal protein synthesis rates are regulated by feedback mechanisms sensitive to the rRNA concentration (5). In each of the seven *rrm* operons in *E. coli*, rRNA is transcribed from two promoters, P1 and P2 (Fig. 1A). Most rRNA transcrip-

tion at moderate to high growth rates originates from the P1 promoters, whose activities increase with growth rate and are thus responsible for regulation (6). Multiple systems affect transcription by *rrm* P1 promoters. Positive effectors include (i) a promoter upstream (UP) element that increases *rrm* P1 activity by binding the α subunit of RNA polymerase (RNAP) (7-9); (ii) a transcription factor, FIS, that binds to sites upstream of the UP element and interacts directly with RNAP (10, 11); and (iii) antitermination factors that bind to the BoxA region in the precursor RNA downstream of *rrm* P2 and prevent premature transcription termination (12). In addition, a negative effector, ppGpp, inhibits transcription from both *rrm* P1 and *rrm* P2 during amino acid starvation, a phenomenon referred to as the stringent response (13-15). Overlapping mechanisms influencing rRNA transcription have complicated efforts to identify the major system (or systems) contributing to growth rate-dependent control.

Previously, we evaluated the contributions of the above mechanisms to growth rate-dependent control of the *rrmB* P1 promoter, using promoter or gene mutations to systematically eliminate specific input signals. Transcription from a "minimal" (core)

T. Gaal, M. S. Bartlett, W. Ross, and R. L. Gourse are in the Department of Bacteriology, University of Wisconsin, 1550 Linden Drive, Madison, WI 53706, USA. C. L. Turnbough Jr. is in the Department of Microbiology, University of Alabama, Birmingham, AL 35294, USA.

*To whom correspondence should be addressed. E-mail: rgourse@bact.wisc.edu